



Cite this article: Roche RC, Heenan A, Taylor BM, Schwarz JN, Fox MD, Southworth LK, Williams GJ, Turner JR. 2022 Linking variation in planktonic primary production to coral reef fish growth and condition. *R. Soc. Open Sci.* **9**: 201012.

<https://doi.org/10.1098/rsos.201012>

Received: 4 June 2020

Accepted: 9 August 2022

Subject Category:

Ecology, conservation and global change biology

Subject Areas:

ecology/environmental science

Keywords:

primary production, coral reef fish, carbon, nitrogen, stable isotope analysis, pelagic energetic subsidies

Author for correspondence:

Ronan C. Roche

e-mail: r.roche@bangor.ac.uk

Electronic supplementary material is available online at <https://doi.org/10.6084/m9.figshare.c.6156452>.

Linking variation in planktonic primary production to coral reef fish growth and condition

Ronan C. Roche¹, Adel Heenan¹, Brett M. Taylor², Jill N. Schwarz³, Michael D. Fox^{4,5}, Lucy K. Southworth^{1,6}, Gareth J. Williams¹ and John R. Turner¹

¹School of Ocean Sciences, Bangor University, Menai Bridge, Anglesey LL59 5AB, UK


²Marine Lab, University of Guam, Mangilao 96923, Guam

³School of Biological and Marine Sciences, University of Plymouth, Plymouth PL4 8AA, UK

⁴Woods Hole Oceanographic Institution, Woods Hole, MA 02543, USA

⁵Red Sea Research Center, King Abdullah University of Science and Technology, Thuwal 23955, Saudi Arabia

⁶Centre of Excellence for Coral Reef Studies, College of Science and Engineering, James Cook University, Douglas, QLD 4811, Australia

 RCR, 0000-0002-6342-9571; JNS, 0000-0002-3589-3887; GJW, 0000-0001-7837-1619

Within low-nutrient tropical oceans, islands and atolls with higher primary production support higher fish biomass and reef organism abundance. External energy subsidies can be delivered onto reefs via a range of physical mechanisms. However, the influence of spatial variation in primary production on reef fish growth and condition is largely unknown. It is not yet clear how energy subsidies interact with reef depth and slope. Here we test the hypothesis that with increased proximity to deep-water oceanic nutrient sources, or at sites with shallower reef slopes, parameters of fish growth and condition will be higher. Contrary to expectations, we found no association between fish growth rate and sites with higher mean chlorophyll-*a* values. There were no differences in fish $\delta^{15}\text{N}$ or $\delta^{13}\text{C}$ values between depths. The relationship between fish condition and primary production was influenced by depth, driven by increased fish condition at shallow depths within a primary production 'hotspot' site. Carbon $\delta^{13}\text{C}$ was depleted with increasing primary production, and interacted with reef slope. Our results indicate that variable primary production did not influence growth rates in planktivorous *Chromis fieldi* within 10–17.5 m depth, but show site-specific variation in reef physical characteristics influencing fish carbon isotopic composition.

1. Introduction

Coral reefs are among the most productive global ecosystems, supporting highly abundant reef organisms and fish biomass, despite occurring within oligotrophic tropical oceans. This productivity paradox has been attributed to diverse processes, such as the uptake and recycling of nutrients between the coral host and their endosymbiotic algae [1], the efficient recycling of dissolved inorganic matter by reef sponges [2] and the presence of nitrogen-fixing cyanobacteria within reef corals [3]. However, the ecological importance and variety of mechanisms that deliver external nutrient subsidies stimulating benthic and planktonic food chains on coral reefs are increasingly recognized [4–7].

The variation in pelagic primary productivity across global coral reefs is strongly linked to the spatial and temporal variability in processes delivering external nutrient subsidies. Terrestrial connectivity is a source of external nutrients, via riverine sources creating broad gradients in nutrient availability [8], or derived from guano produced by resident seabird populations on isolated oceanic atolls [9]. Hydrodynamic connectivity and nutrient input from oceanic water masses can occur when physical mechanisms transport the higher nutrient concentrations present in cooler deep water layers upslope to shallower reefs [10,11].

A variety of related and potentially interacting physical mechanisms, such as upwelling [12], internal waves [11,13] and internal tidal bores [10,14] can transport these deeper waters onto coral reefs. These processes are further influenced by geophysical reef characteristics. For example, reefs with a gradual sloping bathymetry show a greater nearshore enhancement in phytoplankton biomass in atolls and islands across the Pacific [5]. This is thought to be explained by physical processes such as internal waves propagating more easily across shallower reef slopes, but being reflected from steeper slopes [5,15]. Once these cold nutrient-rich waters have reached shallower reef areas, breaking surface waves, wind-driven flow and tides can drive further transport into spur and groove systems [16] or across the reef crest [13]. Geographic location, season and the interactions between transportation mechanisms and variable reef slope and topography [17] all determine which areas of reef are influenced by deep-water nutrients, across scales ranging from metres to kilometres [18–20].

There is interest in how external nutrient inputs on coral reefs could relate to resistance and recovery from coral bleaching events [21,22]. One mechanism is through the ability of mixotrophic corals to favour heterotrophic feeding in response to increased resource availability at greater depth and proximity to allochthonous nutrient sources [23,24]. This coral trophic flexibility has been explained across scales by satellite-derived chlorophyll-*a* estimates, which correlate strongly with primary production throughout the photic zone [5,21]. Whether coral reef fishes exhibit similar flexibility in their feeding strategy in response to variability in primary production is unclear, although Hanson *et al.* [6] showed selective feeding on oceanic zooplankton by planktivorous reef fish. Terrestrial nutrient subsidies delivered by seabirds onto shallow reefs can positively influence reef fish biomass and growth rate [9]. It is likely that the spatial variation in nutrient delivery from deep-water oceanic sources will have similarly important and widespread effects on coral reef fish populations, but empirical evidence of this link is scarce.

Stable isotope ratios in fish tissue can be used to infer reliance on the multiple potential nutrient sources (e.g. terrestrial, deep-water and benthic) driving trophic pathways on a reef [7,25,26] and have been successfully employed to identify feeding zones [27], to detect habitat-level [28], and depth-related differences within food chains [29,30]. In particular, enriched $\delta^{15}\text{N}$ and depleted carbon isotope $\delta^{13}\text{C}$ ratios occur in the tissues of some reef fish with increasing concentrations of oceanic primary production [31,32].

Here we test the hypothesis that with increased depth and proximity to deep-water oceanic allochthonous nutrient sources, fish growth and condition will increase, and this pattern will be further emphasized in areas naturally higher in primary production. Specifically, we predict that planktivorous fish growth rate and condition (tissue lipid content assessed by C:N ratio; [33]) will be positively associated with high mean chlorophyll-*a* values and shallower slopes at reef sites. Additionally, we predict that planktivorous fish collected at greater depths will show enriched $\delta^{15}\text{N}$ and depleted $\delta^{13}\text{C}$ values indicating an increased reliance on primary production derived from deeper oceanic nutrient sources.

2. Methods

2.1. Sampling design

We sampled three atolls within the Chagos Archipelago, central Indian Ocean spanning approximately 170 km of latitude, from the 10 to 26 April 2019. Previous research within the Archipelago found

significantly different planktivorous fish biomass between atolls [34]. Within each atoll, we haphazardly selected six sites located on the seaward reef slopes of the atolls so that sites captured the principal cardinal directions of the atoll's coastline and were separated by at least approximately 1 km. We avoided locating sampling sites at the entrance passes of each atoll where exchange of water between the lagoon and ocean would probably complicate the physical processes driving productivity patterns [24].

2.2. Data and materials collected

To characterize the physical steepness of the reef slope, a transect of depth recordings was collected at each sampling site. The transect was performed with a hand-held depth transponder at each study site perpendicular to the reef slope, starting at approximately 5 m depth, and taking sequential, georeferenced depth readings, (Garmin Montana 650T ± 3 m accuracy). Paired (GPS and depth transponder) readings were taken at approximately 30 s intervals moving offshore until the maximum depth range of the transponder was exceeded (approx. 70 m).

To collect particulate organic matter (POM) and zooplankton samples to determine a characteristic isotopic signature at each site we used the following procedure: seawater (approx. 10 l) was collected from 8 to 10 m depth, while zooplankton were collected from approximately 1 m depth using a net with a mesh size of 200 μm . The net was towed at idle speed (25 hp engine) for 10–15 min per site covering approximately 100–300 m. Both sample types were filtered through pre-combusted (450°C, 5 h) glass fibre filters (GF/F 0.7 μm , Whatman), which were then frozen at -20°C and transported to Woods Hole Oceanographic Institution, USA for storage.

To obtain data on fish growth rates and isotopic signatures, we collected otoliths and tissue samples from a ubiquitous reef-associated planktivorous Indian Ocean species *Chromis fieldi* which feeds on zooplankton, generally within a metre of the reef [35]. Individuals were collected by SCUBA divers using 5% clove oil in ethanol solution and hand nets at two depths categorized as moderate (approx. 17.5 m) and shallow (approx. 10 m). We aimed to collect a maximum of 10 individuals per depth at each site. Fish were euthanized in clove oil solution and kept on ice prior to processing within chilled Ikey-Tek© cool boxes. The total length and fork length of each fish was recorded. Sagittal otoliths from each fish were extracted and stored for later analysis. Tissue samples from one site were damaged during ship movements at sea. The anterior dorsal muscle of each fish was sampled and dried at 60°C , before being frozen and transported to Bangor University, UK for storage.

2.3. Analyses

2.3.1. Stable isotopes

POM and zooplankton samples were thawed, rinsed with dilute HCl (5%) to remove carbonate material and rinsed in deionized water. Samples were dried and 2 mg of material were weighed into tin capsules for analysis. Three replicate samples for $\delta^{13}\text{C}$ and $\delta^{15}\text{N}$ were prepared for POM and zooplankton. Dried fish muscle tissue was ground into a powder and 0.5–1.5 mg of tissue weighed into tin capsules. Isotope $\delta^{13}\text{C}$ and $\delta^{15}\text{N}$ analysis of the collected fish tissue took place at the University of New Mexico Center for Stable Isotopes. Analysis was carried out using a Thermo Scientific Delta V mass spectrometer with a dual inlet and Conflo IV interface connected to a Costech 4010 elemental analyser and a high-temperature conversion elemental analyser.

Isotope values of $\delta^{13}\text{C}$ and $\delta^{15}\text{N}$ were reported using delta notation, in per mil (‰), as deviations from standards (Vienna Pee Dee Belemnite (V-PDB) for $\delta^{13}\text{C}$ and atmospheric N_2 for $\delta^{15}\text{N}$) according to the formula

$$\delta X_{\text{sample}} = \left[\left(\frac{R_{\text{sample}}}{R_{\text{standard}}} \right) - 1 \right] \times 1000,$$

where R_{sample} is the ratio of heavy to light isotope in the sample and R_{standard} is the ratio of heavy to light isotope in the standard. Within-run analytical error assessed via repeated analysis of internal proteinaceous reference materials (Pugel and Acetanilide) was estimated to be $\pm 0.2\text{‰}$ for both $\delta^{13}\text{C}$ and $\delta^{15}\text{N}$.

The ratio of carbon to nitrogen per cent weight in tissue (C:N) from stable isotope analysis was compared among sites as a proxy for tissue lipid content [33]. Lipids are depleted in $\delta^{13}\text{C}$ relative to other tissue types and a positive linear relationship has been established between C:N and lipid content for aquatic animals [36]. If C:N values were above 3.5 [37], isotope $\delta^{13}\text{C}$ values from fish

muscle tissue were corrected for high lipid content using the formula from Post *et al.* [36]

$$\delta^{13}\text{C}_{\text{normalized}} = \delta^{13}\text{C}_{\text{untreated}} - 3.32 + 0.99 \times \text{C:N}.$$

In interpreting our results, two potential sources of variation in $\delta^{13}\text{C}$ and $\delta^{15}\text{N}$ and C:N ratios were tested: (i) a potential influence of fish size on C:N ratio was tested by a linear regression between C:N ratio and FL using all fish samples and (ii) growth effects on $\delta^{13}\text{C}$ and $\delta^{15}\text{N}$ were tested by a linear regression between site level K_{max} and site level $\delta^{13}\text{C}$ and $\delta^{15}\text{N}$ values (electronic supplementary material).

We used $\delta^{13}\text{C}$ and $\delta^{15}\text{N}$ values to characterize an isotopic niche as a proxy for the ecological niche occupied by *Chromis fieldi* across our sampling locations. Isotope niche was estimated by calculating the extent of $\delta^{13}\text{C}$ and $\delta^{15}\text{N}$ in biplot space using the area of standard ellipses estimated by Bayesian inference with the SIBER R package [38]. Standard ellipses (SEA_c) were fitted for fish, POM and zooplankton samples, grouping by atoll and depth, using a 40% confidence interval [38]. The size of ellipses was compared fitting Bayesian models (SEA_b ; 10^4 iterations), differences in standard ellipse area were interpreted graphically, and considered significant when greater than or equal to 95% of posterior draws for one group were smaller than the other [38].

2.3.2. Fish otolith analysis

Otolith microstructure was examined to determine fish growth rate following Taylor *et al.* [39]. One otolith from each pair obtained from individual fish was weighed to the nearest 0.00001 g and attached to a glass microscope slide using thermoplastic glue. Otolith sections were examined on a minimum of two occasions using a dissecting microscope with transmitted light. Ages in years were determined by counting the alternating banding pattern along the dorsal otolith margin. Where ages obtained for an individual differ within these two counts, a third count was performed and the final age was determined by agreement of two separate counts.

Where it was not possible to unequivocally determine placement of the first annuli, or where individuals (probably juveniles or recent recruits) had no clear annual banding pattern, daily growth increments (DGIs) were examined. DGIs were obtained using a compound microscope after successive wet-polishing with 9, 3 and 0.3 μm lapping film, with age in days determined on three separate occasions and the final age was the mean of the three counts. Samples with counts that were outside of 10% of the median were excluded. Parameters of growth were estimated from length-at-age data obtained from all fish collected per site. The von Bertalanffy growth function was used, which is represented by

$$L_t = L_{\infty}[1 - e^{-k(t-t_0)}],$$

in which L_t is the mean predicted fork length (cm) at age t (years) L_{∞} is the mean asymptotic fork length, k is the coefficient used to describe the curvature of fish growth towards L_{∞} and t_0 is the hypothetical age at which FL is equal to zero as described by k .

k was standardized relative to the maximum size of *Chromis fieldi* to obtain K_{max} following Morais and Bellwood [40], and using the formula

$$\log_{10}K_{\text{max}} = \emptyset + s_L \log_{10}L_{\text{max}},$$

in which K_{max} is the expected growth coefficient at the theoretical maximum species size, \emptyset is the growth performance index, s_L is the slope of the relationship between L_{∞} (asymptotic fork length) and k (von Bertalanffy growth parameter), and L_{max} is the maximum reported species size.

2.3.3. Satellite-derived surface chlorophyll-a concentration

Satellite-derived estimates of nearshore primary production were obtained using chlorophyll-a as a proxy for phytoplankton biomass and availability of planktonic food resources. Remotely sensed surface chlorophyll-a values are well correlated with primary production throughout the photic zone in a range of water types and also well correlated with the abundance of zooplankton [41–44]. We used Ocean Land Colour Instrument (OLCI) imagery from the Sentinel-3A and 3B platforms operated by the European Space Agency, augmented by data from the Moderate Resolution Imaging Spectrometer (MODIS) on the Aqua platform operated by NASA, for the period July 2017 to April 2019. This allowed for overlap of the expected collected fish lifespan (we hypothesized based on the size of fish collected, that many spent approximately 2 years since settlement on reefs). Level 1 OLCI

data were acquired from the NASA Ocean Biology Processing Group (oceancolor.gsfc.nasa.gov) and processed to level 2 using the NASA SeaDAS library function l2gen.

2.3.3.1. Satellite data masking procedure

To obtain chlorophyll-a data which were not contaminated with anomalously high chlorophyll-a values associated with altered water column properties in shallow nearshore areas (e.g. bottom reflectance from sand), we created a filtering mask surrounding atolls and removed all pixels inshore of the 30 m isobath *sensu* Gove *et al.* [45] using supervised maximum-likelihood classification of 10 m resolution Sentinel 2 Multi-spectral imager (MSI) data, validated against *in situ* depth sounding data. In the initial Stage 1 submission, we proposed using ETOPO1 bathymetry data [46] to create the 30 m filtering mask, but errors in the ETOPO1 bathymetry were exposed by comparison with *in situ* depth sounding data around islands, and this approach was not used to generate the chlorophyll-a data used in analysis.

2.3.3.2. Site-level satellite data procedure

We validated the resulting chlorophyll-a values in offshore areas (depth greater than 100 m and distance from shore greater than 40 km [47,48] against MODIS-Aqua (1 km spatial resolution) chlorophyll-a [49,50] and against those obtained using shallow water optimization with resolved depth (SWORD) values [51]. We generated annual mean chlorophyll-a maps for the entire study period (2017–2019) and produced spatially integrated chlorophyll-a values for each study site. This was achieved using satellite pixel data matching geographic location to the site, but using a 3×3 pixel box (300 m OLCI spatial resolution) excluding any depth-masked pixels, giving site level mean and s.d. estimates.

2.4. Statistical analysis

To test for associations between the growth and condition of fish and potential variability in deep water nutrient input, we constructed generalized linear models. Models were fitted to each of the following response variables separately: fish growth rate (K_{\max}), fish condition (C:N ratio) and isotopic value ($\delta^{13}\text{C}$ and $\delta^{15}\text{N}$). All models included atoll (three levels) and collection depth (two levels) as categorical independent variables (fixed factors), together with the continuous independent variables of site chlorophyll-a and reef slope. We examined for interactions between: depth of collection and mean chlorophyll-a, depth of collection and site slope, and mean chlorophyll-a and site slope, for each response variable. The Benjamini–Hochberg method was used to correct for multiple testing, using a false discovery rate of 10% [52].

To further examine whether fish growth rate (K_{\max}), fish condition (C:N ratio), $\delta^{13}\text{C}$ and $\delta^{15}\text{N}$ values differ between collection depths, we used permutation testing to randomly reassign blocks of sites between depths. This tested for a difference in sample means associated with the depth of sample collection (using an alpha value of 0.05) in fish growth rate (K_{\max}), fish condition (C:N ratio), $\delta^{13}\text{C}$ and $\delta^{15}\text{N}$ values.

The specific hypotheses that were tested within this framework, together with the simulated power (from modelPower R function for glm models, and 999 simulations within the emon R package for permutation tests) for each dataset and analysis method, are shown in the design table (table 1).

3. Results

We carried out sample data collection and analysis according to the in-principle accepted Stage 1 protocol. The final dataset consisted of size and otolith measurements from 288 *Chromis fieldi* individuals, and paired isotope data from 284 individuals (four samples were damaged during mass spectrometer analysis). Supporting isotopic characterization data consisted of 13 POM samples and 22 pelagic zooplankton samples (<https://osf.io/6wjsq/>).

3.1. Isotopic niche area

The relative trophic position of all taxa was visualized within an isoscape of $\delta^{15}\text{N}$ and $\delta^{13}\text{C}$ values (figure 1). Standard Bayesian ellipse areas (SEA_c) fitted showed clear segregation between main trophic groups (POM, zooplankton and fish: figure 1*a*). There was a small overlap in isotope space between the SEA_c of zooplankton and POM (figure 1*a*). The SEA_c of fish collected at shallow (10 m)

Table 1. Registered report design table listing study hypotheses.

hypothesis	power analysis	statistical test	interpretation given different outcomes	test result
H1 fish growth rate is increased at sites with higher mean chlorophyll- <i>a</i> values	power = 0.81 effect size $p\text{Eta}^2 = 0.23$	regression coefficient from generalized linear model	we used the p -value for the chl- <i>a</i> regression coefficient to test for evidence that variation in primary production around atolls influences planktivorous fish growth rate	not supported
H2 fish condition (C : N ratio is higher (indicating higher lipid content) at sites with higher mean chlorophyll- <i>a</i>)	power = 0.99 effect size $p\text{Eta}^2 = 0.58$	regression coefficient from generalized linear model	we used the p -value for the chl- <i>a</i> regression coefficient to test for evidence that variation in primary production around atolls influences planktivorous fish condition	not supported
H3 fish nitrogen isotope ($\delta^{15}\text{N}$) values depleted at sites with higher mean chlorophyll- <i>a</i>	power = 0.88 effect size $p\text{Eta}^2 = 0.3$	regression coefficient from generalized linear model	we used the p -value for the chl- <i>a</i> regression coefficient to test for evidence that variation in primary production around atolls influences planktivorous fish ($\delta^{15}\text{N}$)	not supported
H4 fish carbon isotope values ($\delta^{13}\text{C}$) values will be enriched at sites with higher mean chlorophyll- <i>a</i>	power = 0.99 effect size $p\text{Eta}^2 = 0.5$	regression coefficient from generalized linear model	we used the p -value for the chl- <i>a</i> regression coefficient to test for evidence that variation in primary production around atolls influences planktivorous fish ($\delta^{13}\text{C}$)	supported
H5 fish growth rate is higher at sites with gradual reef slopes facilitating physical delivery mechanisms	power = 0.81 effect size $p\text{Eta}^2 = 0.23$	regression coefficient from generalized linear model	we used the p -value for the reef slope regression coefficient to test for evidence that variable delivery of nutrients with reef slope around atolls influences planktivorous fish growth	not supported
H6 fish condition (C : N ratio) is increased indicating higher lipid content with gradual reef slopes facilitating physical nutrient delivery mechanisms	power = 0.91 effect size $p\text{Eta}^2 = 0.29$	regression coefficient from generalized linear model	we used the p -value for the reef slope regression coefficient to test for evidence that variable delivery of nutrients with reef slope around atolls influences planktivorous fish condition	not supported
H7 fish nitrogen isotope ($\delta^{15}\text{N}$) will be enriched with gradual reef slopes facilitating physical nutrient delivery mechanisms	power = 0.92 effect size $p\text{Eta}^2 = 0.3$	regression coefficient from generalized linear model	we used the p -value for the reef slope regression coefficient to test for evidence that variable delivery of nutrients with reef slope around atolls influences planktivorous fish $\delta^{15}\text{N}$	not supported
H8 fish carbon isotope values ($\delta^{13}\text{C}$) will be depleted with gradual reef slopes facilitating physical nutrient delivery mechanisms	power = 0.99 effect size $p\text{Eta}^2 = 0.78$	regression coefficient from generalized linear model	we used the p -value for the reef slope regression coefficient to test for evidence that variable delivery of nutrients with reef slope around atolls influences planktivorous fish ($\delta^{13}\text{C}$)	not supported (direction reversed)
H9 the relationship between fish growth rate and site chlorophyll- <i>a</i> values is influenced by depth of collection (moderate versus shallow)	power = 0.85 effect size $p\text{Eta}^2 = 0.25$	regression coefficient from generalized linear model	we used the p -value for the reef slope regression coefficient to test for evidence that depth influences the relationship between chl- <i>a</i> and fish growth rate	not supported

(Continued.)

Table 1. (Continued.)

hypothesis	power analysis	statistical test	interpretation given different outcomes	test result
H10 The relationship between fish condition (C : N ratio) and site chlorophyll- <i>a</i> values is influenced by depth of collection (moderate versus shallow)	power = 0.85 effect size $p\text{Eta}^2 = 0.25$	regression coefficient from generalized linear model	we used the <i>p</i> -value for the regression interaction coefficient to test for evidence that depth influences the relationship between chl- <i>a</i> and fish C : N ratio	supported
H11 the relationship between fish nitrogen isotope ($\delta^{15}\text{N}$) and site chlorophyll- <i>a</i> values is influenced by depth of collection (moderate versus shallow)	power = 0.85 effect size $p\text{Eta}^2 = 0.27$	regression coefficient from generalized linear model	we used the <i>p</i> -value for the regression interaction coefficient to test for evidence that depth influences the relationship between chl- <i>a</i> and fish ($\delta^{15}\text{N}$)	not supported
H12 the relationship between fish ($\delta^{13}\text{C}$) and site chlorophyll- <i>a</i> values is influenced by depth of collection (moderate versus shallow)	power = 0.82 effect size $p\text{Eta}^2 = 0.25$	regression coefficient from generalized linear model	we used the <i>p</i> -value for the regression interaction coefficient to test for evidence that depth influences the relationship between chl- <i>a</i> and fish ($\delta^{13}\text{C}$)	not supported
H13 the relationship between fish growth rate and reef site slope is influenced by depth of collection (moderate versus shallow)	power = 0.81 effect size $p\text{Eta}^2 = 0.23$	regression coefficient from generalized linear model	we used the <i>p</i> -value for the regression interaction coefficient to test for evidence that depth influences the relationship between reef slope and growth rate	not supported
H14 the relationship between fish condition (C : N ratio) and reef site slope is influenced by depth of collection (moderate versus shallow)	power = 0.85 effect size $p\text{Eta}^2 = 0.25$	regression coefficient from generalized linear model	we used the <i>p</i> -value for the regression interaction coefficient to test for evidence that depth influences the relationship between reef slope and C : N ratio	not supported
H15 fish nitrogen isotope ($\delta^{15}\text{N}$) and reef site slope is influenced by depth (moderate versus shallow)	power = 0.88 effect size $p\text{Eta}^2 = 0.29$	regression coefficient from generalized linear model	we used the <i>p</i> -value for the regression interaction coefficient to test for evidence that depth influences the relationship between reef slope and ($\delta^{15}\text{N}$)	not supported
H16 the relationship between fish carbon isotope ($\delta^{13}\text{C}$) and reef site slope is influenced by depth (moderate versus shallow)	power = 0.85 effect size $p\text{Eta}^2 = 0.25$	regression coefficient from generalized linear model	we used the <i>p</i> -value for the regression interaction coefficient to test for evidence that depth influences the relationship between reef slope and ($\delta^{13}\text{C}$)	not supported
H17 the relationship between fish growth rate and site chlorophyll- <i>a</i> is influenced by reef site slope	power = 0.81 effect size $p\text{Eta}^2 = 0.23$	regression coefficient from generalized linear model	we used the <i>p</i> -value for the regression interaction coefficient to test for evidence that slope influences the relationship between chl- <i>a</i> and fish growth rate	not supported
H18 the relationship between fish condition (C : N ratio) and site chlorophyll- <i>a</i> is influenced by reef site slope	power = 0.85 effect size $p\text{Eta}^2 = 0.25$	regression coefficient from generalized linear model	we used the <i>p</i> -value for the regression interaction coefficient to test for evidence that slope influences the relationship between chl- <i>a</i> and fish C : N ratio	not supported

(Continued.)

Table 1. (Continued.)

hypothesis	power analysis	statistical test	interpretation given different outcomes	test result
H19 the relationship between fish nitrogen ($\delta^{15}\text{N}$) values and site chlorophyll-a is influenced by reef site slope	power = 0.88 effect size $f^2 = 0.29$	regression coefficient from generalized linear model	we used the p -value for the regression interaction coefficient to test for evidence that slope influences the relationship between chl-a and fish ($\delta^{15}\text{N}$)	not supported
H20 the relationship between fish ($\delta^{13}\text{C}$) values and site chlorophyll-a is influenced by reef site slope	power = 0.85 effect size $f^2 = 0.25$	regression coefficient from generalized linear model	we used the p -value for the regression interaction coefficient to test for evidence that slope influences the relationship between chl-a and fish ($\delta^{13}\text{C}$)	not supported
H21 fish growth rate is higher in fish collected at moderate versus shallow depths	power = 0.80 effect size $d = 27\%$	permutation test between groups ($\alpha = 0.05$)	we used the p -value from permutation testing the probability that the null hypothesis of no difference is true	not supported
H22 fish C : N ratio will be higher within fish collected at moderate versus shallow depths	power = 0.83	permutation test between groups ($\alpha = 0.05$)	we used the p -value from permutation testing the probability that the null hypothesis of no difference is true	not supported
H23 fish nitrogen ($\delta^{15}\text{N}$) values will be depleted within in fish collected at moderate versus shallow depths	effect size $d = 0.15$ power = 0.80 effect size $d = 0.3$	permutation test between groups ($\alpha = 0.05$)	we used the p -value from permutation testing the probability that the null hypothesis of no difference is true	not supported
H24 fish carbon isotope values ($\delta^{13}\text{C}$) will be depleted within in fish collected at moderate versus shallow depths	power = 0.82 effect size $d = 0.2$	permutation test between groups ($\alpha = 0.05$)	we used the p -value from permutation testing the probability that the null hypothesis of no difference is true	not supported

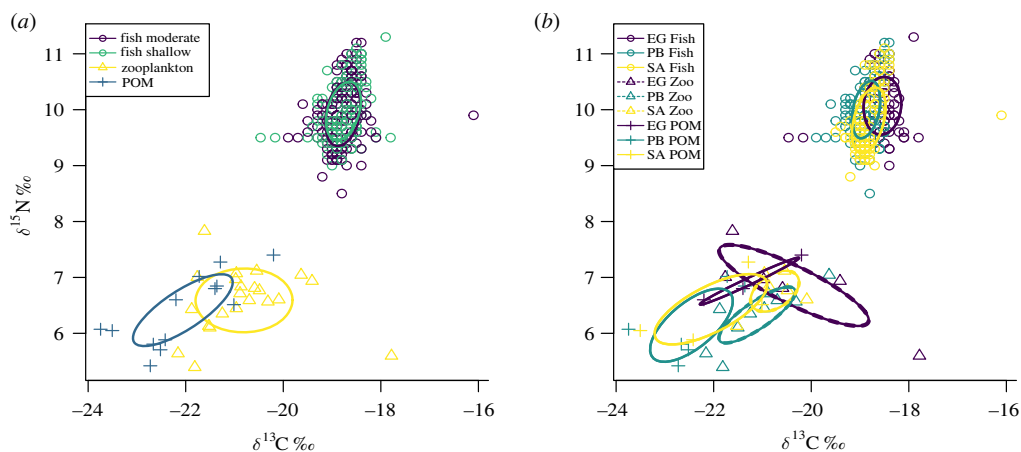


Figure 1. Stable isotope biplot of POM, zooplankton and *Chromis fieldi*, (a) SEA_c for fish collected at shallow and moderate depth, (b) SEA_c for each taxa by atoll.

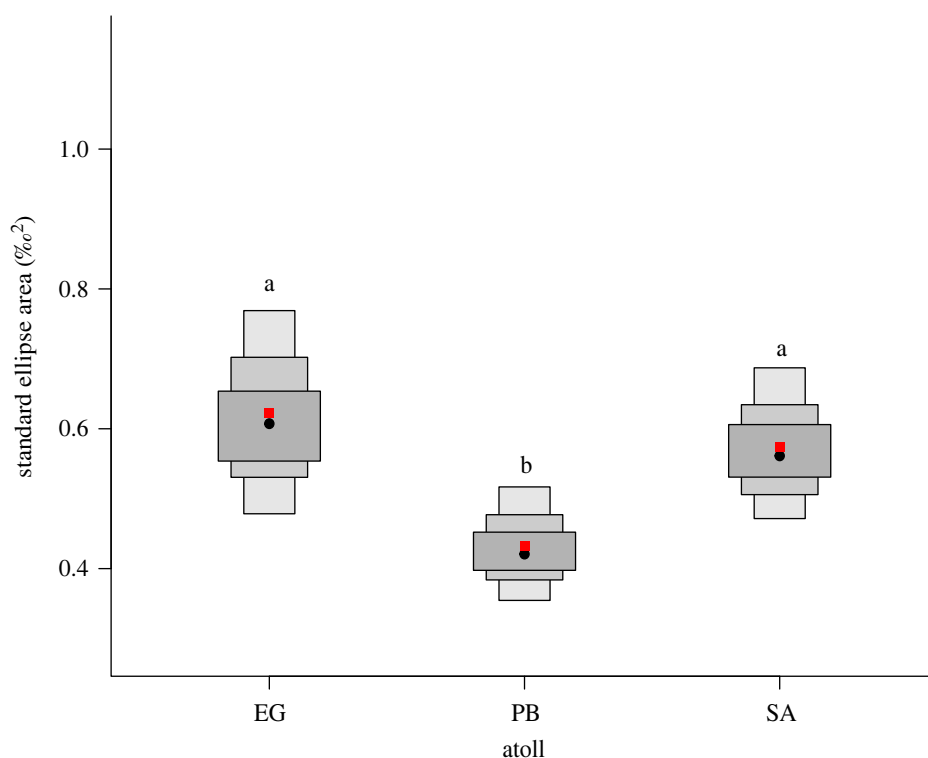


Figure 2. Density plots of SEA_b of *Chromis fieldi* by atoll. The population mode is shown by a black dot and boxes of increasing size and colour represent 50%, 75% and 95% credible intervals; the red square represents the SEA_c corrected for sample size according to Jackson *et al.* [38]. Common letters denote no significant difference according to Bayesian inference ($p > 0.05$).

and moderate depths (17.5 m) were closely aligned and occupied a similar position within the isoscape (figure 1a). Differences between atolls were apparent in the position of the fish SEA_c , mainly along the $\delta^{13}\text{C}$ axis (figure 1b). Differences in the position and size of the zooplankton SEA_c were present between atolls, with the largest SEA at Egmont Atoll (EG) (figure 1b). The SEA_c for POM overlapped between Salomon Atoll (SA) and Peros Banhos Atoll (PB), and to a lesser extent for Egmont Atoll (figure 1b).

Between atolls, the probability for the posterior distribution (based on 10 000 draws) that planktivorous fish sampled from Egmont Atoll occupied a greater isotopic niche area than Peros Banhos Atoll was 99.2% (figure 2). The probability that fish sampled from Egmont atoll occupied a greater isotopic niche area than from Salomon Atoll was 68%. The probability that fish sampled from Salomon atoll occupied a larger isotopic niche area than from Peros Banhos Atoll was 98% (figure 2).

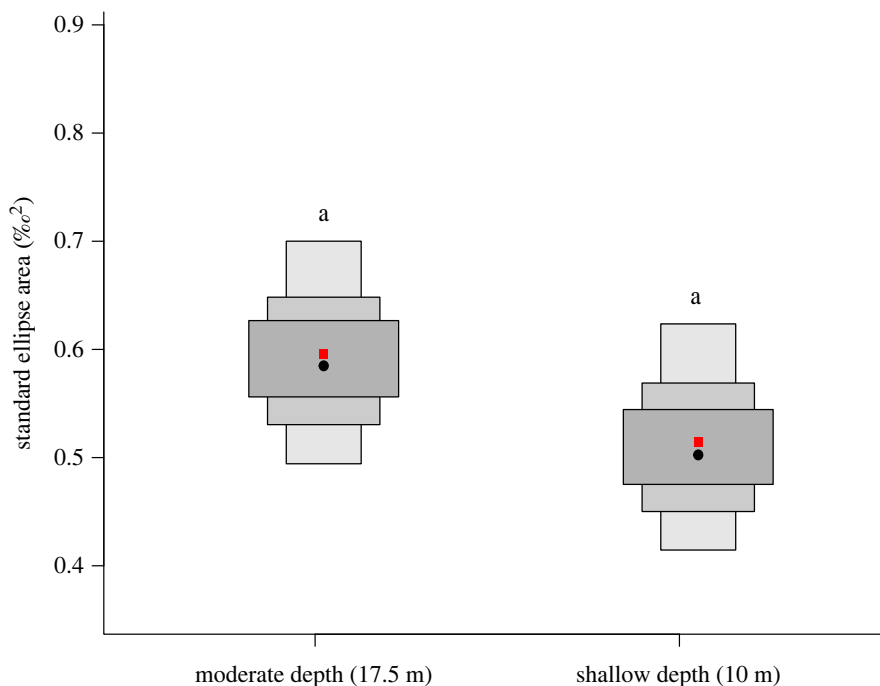


Figure 3. Density plots of $SEAb$ of *Chromis fieldi* by depth. The population mode is shown by a black dot and boxes of increasing size and colour represent 50%, 75% and 95% credible intervals; the red square represents the $SEAc$ corrected for sample size according to Jackson *et al.* [38]. Common letters denote no significant difference according to Bayesian inference ($p > 0.05$).

Between depths, the probability for the posterior distribution that fish sampled from moderate depths occupied a larger isotopic niche was 87% (figure 3). Comparing depth by atoll, the probability that fish occupied a larger isotopic niche at shallow than at moderate depth was 100% for Egmont Atoll (figure 4). The probability that fish occupied a larger isotopic niche at moderate, relative to shallow depth was 0% for Peros Banhos Atoll, and 99.9% for Salomon Atoll (figure 4).

3.2. Fish condition

The metric of fish condition (C : N ratio) obtained from fish muscle tissue samples ranged from 2.9 to 4.7 for each individual. The regression between fish size and condition showed a weak but significant relationship ($R^2 = 0.12$, $F_{1,265} = 36.27$, $p \leq 0.001$; electronic supplementary material, table S2), indicating that as fish size increased, condition decreased.

3.3. Fish size and growth rate influence on isotope data

Measurements of total length of *Chromis fieldi* collected ranged from 17 to 70 mm. Site- and depth-specific von Bertalanffy growth curves were obtained and K_{max} standardized growth rate calculated from 27 of a possible total of 36 site-depth combinations (nine site-depth samples had insufficient sample size or no growth curve fit was possible; electronic supplementary material, figures S4–S6). The regression between K_{max} and carbon isotope values was not significant ($R^2 = 0.01$, $F_{1,25} = 0.26$, $p = 0.62$). There was a significant relationship between K_{max} and nitrogen isotope values ($R^2 = 0.48$, $F_{1,25} = 23.26$, $p < 0.001$; electronic supplementary material, table S3 and figure S7), indicating that as K_{max} increased, $\delta^{15}N$ values were depleted.

3.4. Satellite-derived chlorophyll-a and reef slope data

Reef slope data were obtained from 16 of 18 *in situ* stations and reef slope angles ranged from -16 to -70 degrees (<https://osf.io/6wjsq/>). Sentinel-3A/B OLCI surface chlorophyll-a data were obtained from 3×3 pixel boxes (300 m spatial resolution) for 16 of 18 *in situ* stations and were time-averaged over the period July 2017 to August 2019 (figure 5a). Results of the masking procedure using supervised maximum-likelihood habitat classification of Sentinel MSI data validated with *in situ* reef profiles are

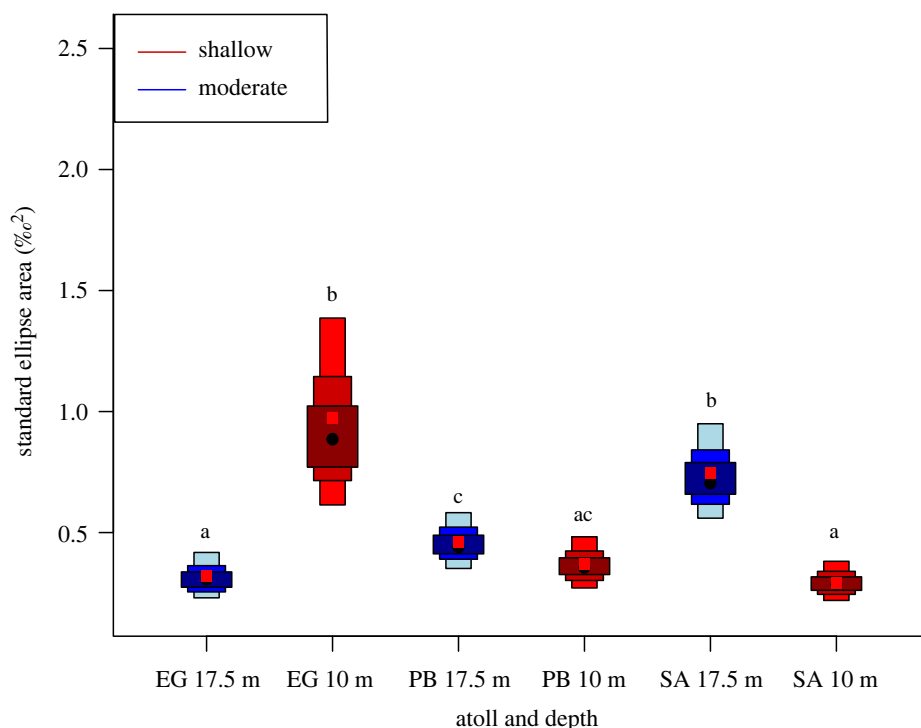


Figure 4. Density plots of SEA_b of *Chromis fieldi* by atoll and depth. The population mode is shown by a black dot and boxes of increasing size and colour represent 50%, 75% and 95% credible intervals; the red square represents the SEA_c corrected for sample size according to Jackson *et al.* [38]. Common letters denote no significant difference according to Bayesian inference ($p > 0.05$).

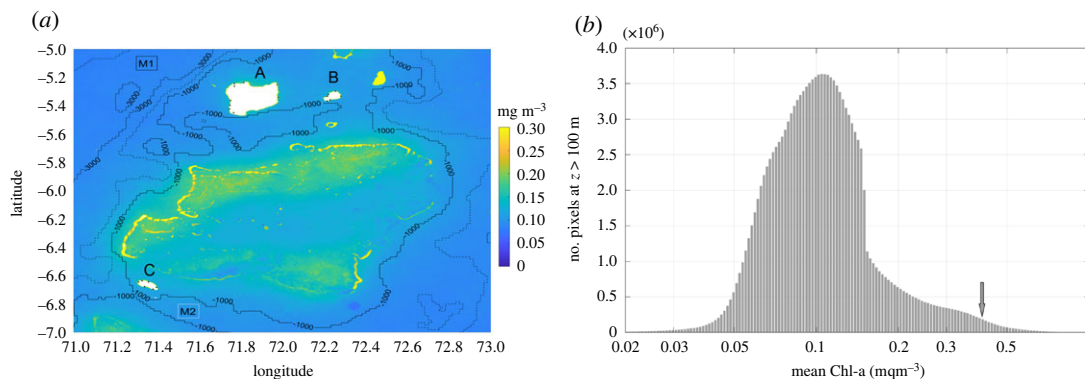


Figure 5. (a) Time-averaged (July 2017–August 2019) chlorophyll-*a* from Sentinel 2 and 3 OLCI. Depth contours are taken from ETOPO-1 [46]. Boxes M1 and M2 are the regions in greater than 1000 m depth chosen for comparison against MODIS-Aqua. Atolls (A) Peros Banhos, (B) Salomon and (C) Egmont are masked using Sentinel 2 MSI masks. (b) Frequency histogram of time-averaged chlorophyll-*a* (excluding areas shallower than 100 m) for the study domain shown within (a). The value of the highest chlorophyll-*a* site sampled at Egmont Atoll is indicated by an arrow within this histogram.

shown for Egmont Atoll (figure 6) and Salomon and Perhos Banhos Atolls (electronic supplementary material, figures S9 and S10). Mean chlorophyll-*a* across all 16 sites was $0.148 \pm 0.068 \text{ mg m}^{-3}$. Mean chlorophyll-*a* values were higher at sites located around Egmont Atoll ($0.211 \pm 0.12 \text{ mg m}^{-3}$) than Salomon Atoll ($0.129 \pm 0.006 \text{ mg m}^{-3}$) and Peros Banhos Atoll ($0.123 \pm 0.004 \text{ mg m}^{-3}$). Across all three atolls, site chlorophyll-*a* ranged from 0.116 to 0.405 mg m^{-3} . The highest site chlorophyll-*a* values from the northern section of Egmont Atoll ('Egmont Mid': 0.405 mg m^{-3}) were at least two times greater than all other sites; however, satellite data processing showed no indication that this site was more likely to be influenced by issues of reef glint or bottom reflectance than others within the dataset and found consistently high temporal variability at this site (electronic supplementary material, figure S17). A histogram of time-averaged chlorophyll-*a* values within the study domain at

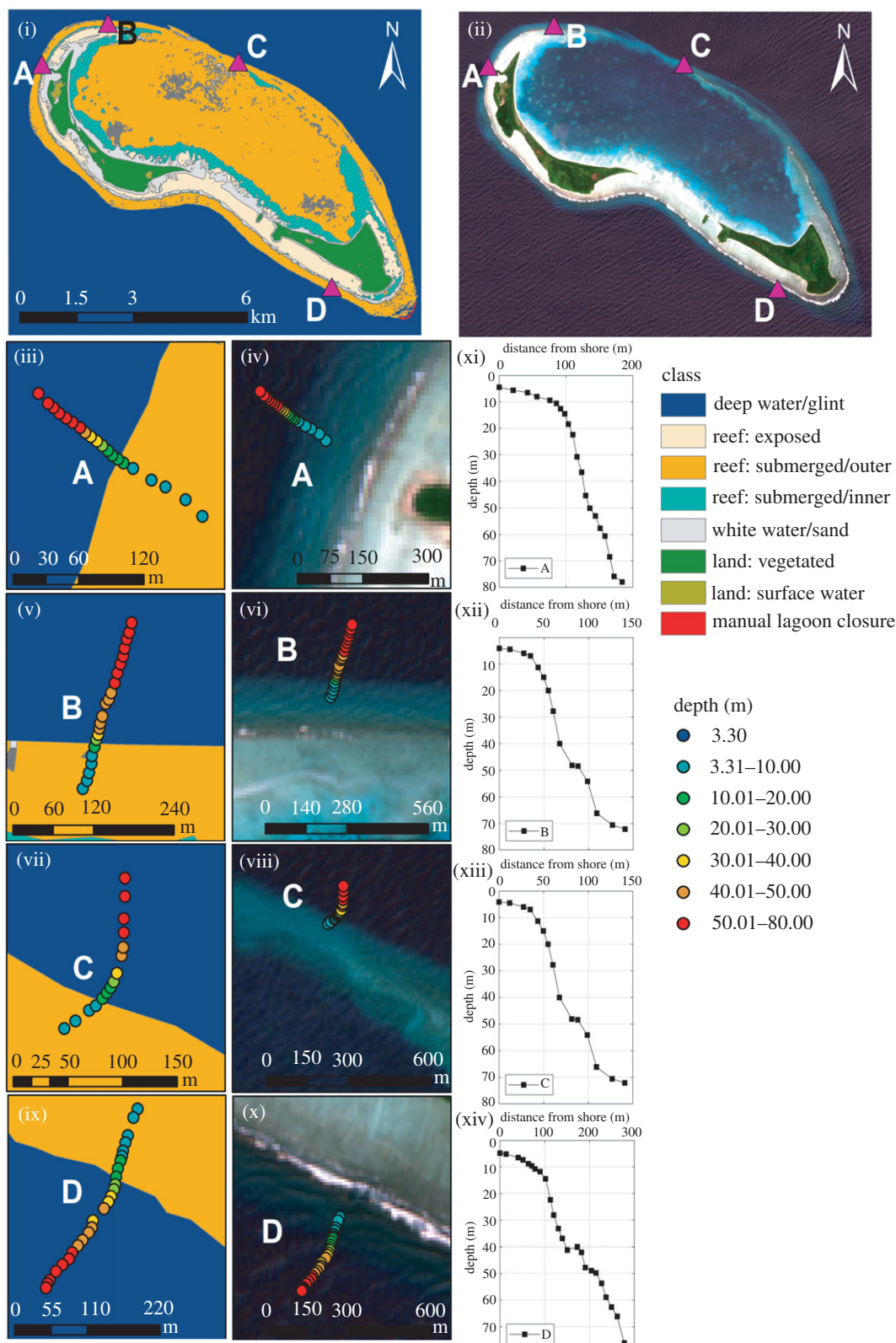


Figure 6. (i) Habitat masking map produced from Sentinel 2 MSI data for Egmont Atoll, (ii) reef slope site locations (A, B, C, D) around Egmont Atoll, (iii, v, vii, ix) sites A, B, C, D *in situ* depth soundings plotted on habitat masking map, (iv, vi, viii, x) sites A, B, C, D *in situ* depth soundings plotted on Sentinel satellite imagery, (xi, xii, xiii, xiv) reef profiles obtained from *in situ* depth soundings of sites A, B, C, D.

300 m spatial resolution (excluding areas shallower than 100 m), showed values were mainly distributed between 0.05 and 0.17 mg m^{-3} (figure 5b), with a long tail of higher chlorophyll-a values extending from 0.17 to greater than 0.5 mg m^{-3} (figure 5b).

Table 2. Summary of generalized linear model results. Values in parentheses are coefficient standard errors.

	dependent variable:			
	dN	dC	CN	K_{\max}
	normal	normal	normal	gamma
	nitrogen	carbon	C : N ratio	K_{\max}
	(1)	(2)	(3)	(4)
constant	9.831*** (0.284)	-18.622*** (0.081)	3.259*** (0.033)	0.733*** (0.211)
depth	0.086 (0.137)	0.039 (0.039)	0.001 (0.016)	-0.038 (0.098)
slope	-0.771 (0.587)	-0.503*** (0.167)	-0.044 (0.067)	-0.292 (0.466)
Chl-a	-9.446 (6.693)	-5.289** (1.905)	-0.204 (0.768)	-3.727 (5.494)
depth : slope	-0.120 (0.231)	0.032 (0.066)	0.037 (0.026)	-0.007 (0.261)
depth : Chl-a	-1.690 (2.007)	-1.340 (0.571)	1.104*** (0.230)	1.069 (1.431)
slope : Chl-a	-38.602 (25.279)	-20.149** (7.195)	-0.352 (2.900)	-15.214 (20.688)
observations	30	30	30	26
log likelihood	-8.791	28.906	56.165	1.089
Akaike inf. crit.	35.582	-39.811	-94.330	15.821

Note: * $p < 0.1$; ** $p < 0.05$; *** $p < 0.01$.

3.5. Primary production

Hypotheses 1 to 4 tested for relationships between primary production (chlorophyll-a), and fish isotopic composition, condition and growth (table 1). Fish carbon isotope $\delta^{13}\text{C}$ values were depleted at sites with higher mean chlorophyll-a values indicated by a significant negative effect of the chlorophyll-a variable within the carbon isotope linear regression model ($B = -5.29$, s.e. = 1.90, $t = -2.78$, $p = 0.011$; table 2). Hypotheses 1 to 3 were unsupported by the data, and hypothesis 4 was supported (table 1).

3.6. Reef slope

Hypotheses 5 to 8 tested for relationships between reef slope and fish isotopic composition, condition and growth. Hypotheses 17 to 20 tested for interactions between reef slope, chlorophyll-a and fish isotopic composition, condition and growth (table 1). The relationship between fish carbon isotope $\delta^{13}\text{C}$ and reef site chlorophyll-a was influenced by reef site slope, indicated by a significant interaction effect within the carbon isotope regression model ($B = -20.15$, s.e. = 7.19, $t = -2.8$, $p = 0.011$; figure 7). Fish carbon isotope $\delta^{13}\text{C}$ values were depleted with increasing reef slope, indicated by a significant effect of slope within the carbon isotope regression model (table 2). The direction of this effect was reversed compared with the hypothesis of depleted $\delta^{13}\text{C}$ values with gradual slopes (table 1). Hypotheses 5 to 8, and 17 to 19 were unsupported by the data and hypothesis 20 was supported (table 1).

3.7. Depth

Hypotheses 9 to 16, and 21 to 24 tested for relationships between depth and fish isotopic composition, condition and growth (table 1). The relationship between fish condition and site chlorophyll-a was

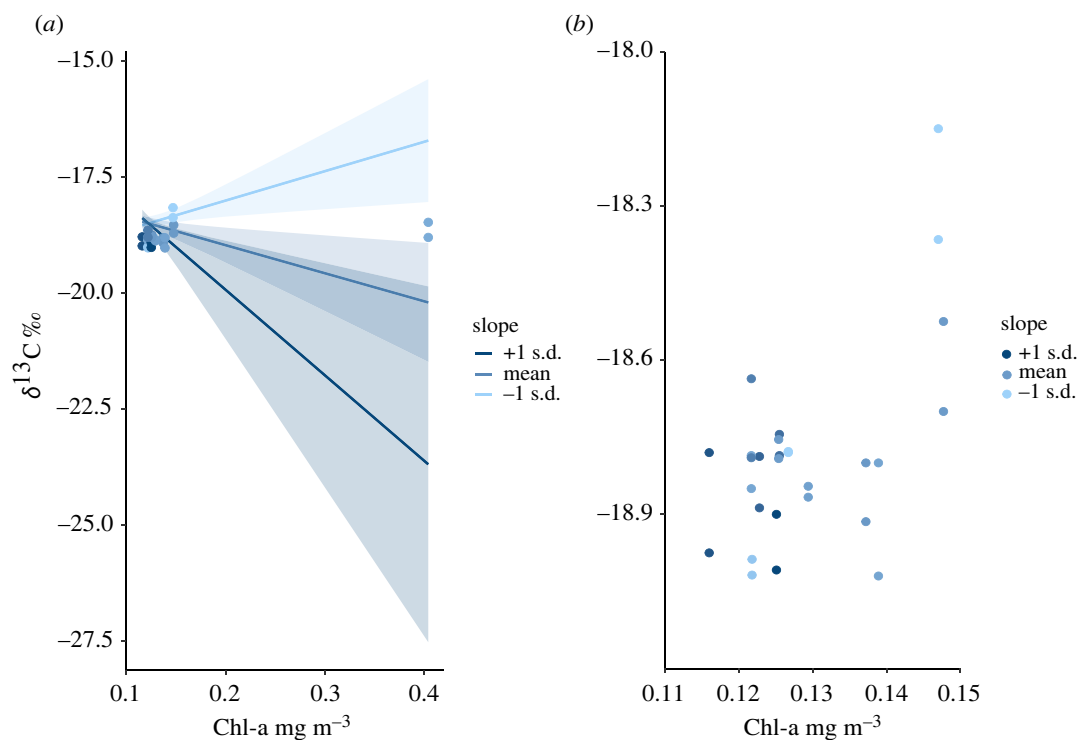


Figure 7. Relationships between planktivorous damselfish carbon isotope $\delta^{13}\text{C}$ and satellite-derived reef site chlorophyll-a values influenced by steepness of reef slope (a) using all sites within the dataset and (b) removing the highest site-level mean chlorophyll-a value.

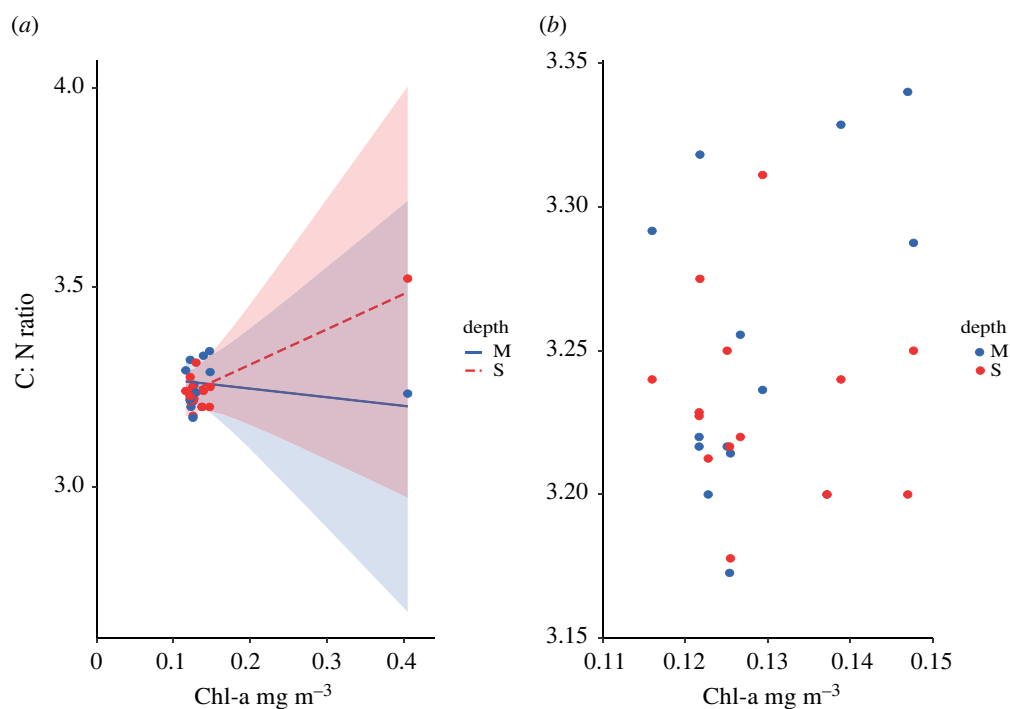


Figure 8. Relationships between planktivorous damselfish condition (C:N ratio) and satellite-derived reef site chlorophyll-a values influenced by the depth of collection: shallow (10 m) versus moderate (17.5 m), (a) using all sites within the dataset and (b) removing the highest site-level mean chlorophyll-a value.

influenced by the depth of collection, indicated by a significant interaction effect within the fish condition (C:N) regression model ($B = 1.11$, s.e. = 0.23, $t = 4.8$, $p \leq 0.001$; figure 8). Hypothesis 9, and 11 to 16 were unsupported by the data (table 1). Hypothesis 10 was supported (table 1). Hypotheses 21 to 24 were

unsupported. There were no significant differences in mean values of fish growth rate, fish condition, fish nitrogen isotope values or fish carbon isotope values when data from shallow and moderate depth collection sites were pooled together and permuted 9999 times between depths (<https://osf.io/6wjsq/>).

4. Discussion

We examined the effect of depth, variation in primary production and reef slope on $\delta^{15}\text{N}$, $\delta^{13}\text{C}$, growth rate and condition of planktivorous fish across 18 sites in the central Indian Ocean. We found no difference in mean isotopic value, growth rate or condition between fish grouped by depth of collection. There was an interactive effect of depth and primary production on fish condition, and an interactive effect of reef slope and primary production on fish $\delta^{13}\text{C}$ values. These interactions were driven by high primary production values present at one study site. In the paragraphs below, we first discuss the absence of an effect of depth on fish growth and condition. Second, we examine the interactive effects of primary production, and the distribution of chlorophyll-*a* values within the study domain. Third, we interpret relationships between fish size and condition, and the effect of growth rate on fish isotope values. Fourth, we draw inferences from isotopic niche area analysis. Finally, we discuss limitations of the present study and suggest data collection methods to strengthen further research on the effects of deep water nutrient inputs to coral reef planktonic food chains.

We hypothesized that planktivorous fish collected at greater depths would exhibit enriched $\delta^{15}\text{N}$ values, consistent with previous findings in the central Pacific [24] and Western Australia [31]. Contrary to our prediction, we did not find a simple depth-dependent pattern within fish $\delta^{15}\text{N}$ values, which suggests that site-specific processes and characteristics unrelated to depth influence fish $\delta^{15}\text{N}$. Alternatively the depth range sampled (10–17.5 m) was insufficient to detect an effect of deep-water nutrient inputs. Our original hypothesis assumes that the zooplankton communities which planktivorous fish consume differ in $\delta^{15}\text{N}$ between depths due to proximity to nutrient delivery from deep water oceanic sources. There are several instrumental datasets, which, while limited in spatial and temporal resolution, suggest movement of colder water from depth to shallow reefs within the Chagos Archipelago [53,54]. Therefore, rather than an absence of these processes across the study sites, the most likely explanation for the lack of a $\delta^{15}\text{N}$ pattern is that zooplankton are influenced by a common oceanic $\delta^{15}\text{N}$ source across sites and that the water column and zooplankton communities are well-mixed across sampled depths. A lack of spatial difference in $\delta^{15}\text{N}$ within planktivorous fish sampled between locations with varying oceanic influence has previously been observed and attributed to similarity in food chain length between locations [25,28].

We also found no significant effect of depth, primary production or reef slope on fish growth rates. This indicates *Chromis fieldi* growth at these sites is not limited by zooplankton availability and that gradients in zooplankton abundance, or variable reef bathymetry between sites did not translate into fish growth rate differences. An increase in the abundance of planktivorous fishes, peaking at moderate (20–30 m) and mesophotic (40–70 m) depths has been widely documented [29,55,56], but evidence for associated growth rate differences across depth gradients on coral reefs is lacking. Contrary to our hypothesis of increasing fish growth rate with proximity to deep water nutrient sources, slower growth trajectories have been found in planktivorous damselfish collected at mesophotic (60–70 m), relative to shallow depths (10 m) at sites in the Florida Keys [57]. The absence of growth rate differences within our study species suggests a lack of response to primary production gradients. Similar spatially invariable growth patterns in spite of strong gradients of chlorophyll-*a* (mean chlorophyll-*a* of 0.79 mg m⁻³ within the Gulf of Aden versus 0.16 mg m⁻³ in the Northern Red Sea) occur within butterflyfish species across the Red Sea region [58].

There was an interactive effect of depth and primary production on fish condition (C:N ratio). At sites with higher primary production, fish condition was higher at shallower depths (figure 8*a*). The higher fish C:N ratios recorded within shallow depths at high primary productivity sites were probably driven by fine-scale oceanographic processes occurring at one of the three study atolls (Egmont Atoll), which contained sites with the highest mean chlorophyll-*a* values. Indeed, when the site with notably high chlorophyll-*a* is removed, there is no significant relationship between C:N ratio, chlorophyll-*a* values and depth (figure 8*b*). Overall, this indicates that planktivorous fish condition does not vary across the range of chlorophyll-*a* values (0.11–0.147 mg m⁻³) in the remaining study sites, which fall within the most frequent mean chlorophyll-*a* concentrations in the study domain (figure 5*b*).

The implications of these findings are notable on two levels. First and most specifically, the sites surveyed at Egmont Atoll appear anomalous and worthy of further investigation. This atoll has a partially enclosed lagoon, which is connected to the adjacent reef slope by a shallow (approx. 5 m) permanently submerged atoll rim along its northern margin. High localized zooplankton abundances have been detected at this location using acoustic backscatter [54]. These have been attributed to a process in which cold water bores transport zooplankton from depth (greater than 50 m) and into the lagoon on flood tides, where they are aggregated before being pumped out across the rim at shallow depths [54]. This is consistent with the higher planktivorous fish condition found at shallow depths on the northern section of the atoll. Second, and more generally, here we sampled sites within a broad but right-skewed distribution of chlorophyll-a values and found no evidence of a mechanistic link between high primary production and planktivorous fish growth or condition, only potentially on the extreme end. This suggests that using the Chagos Archipelago to establish 'baseline or benchmark' values for Indian Ocean coral reef fish biomass [59–61] may not capture the full influence of primary production gradients on fish populations unless sampling site selection for baseline estimates are stratified by this distribution [62].

Fish $\delta^{13}\text{C}$ isotope values were depleted at sites with higher mean chlorophyll-a values, consistent with expectations based on a reliance on primary production derived from deeper oceanic nutrient sources. This difference in $\delta^{13}\text{C}$ with higher mean chlorophyll-a was influenced by an interaction with reef slope (figure 7a). At mean reef slope values, and at reef slopes higher than the mean, fish $\delta^{13}\text{C}$ was depleted with increasing primary production. At shallow reef slopes below the mean, $\delta^{13}\text{C}$ isotope values were enriched with increasing primary production. While influenced by the high chlorophyll-a values present at the Egmont Atoll site, the relationship remains if this site is removed from the dataset (figure 7b). The interaction between reef slope and chlorophyll-a suggests that planktivore $\delta^{13}\text{C}$ values are driven by site-specific characteristics across this study domain. Isotopically distinct planktonic carbon pathways (nearshore reef-associated plankton and offshore pelagic plankton) identified using compound-specific approaches [63], illustrate the complexity underlying bulk fish $\delta^{13}\text{C}$ as obtained here, and the potential importance of interactions between reef slope and hydrodynamic processes affecting the strength of co-occurring carbon isotope pathways.

We found a weak negative relationship between fish size and condition, indicating that smaller fish tended to have higher condition (electronic supplementary material, table S2). This suggests that while fish size is not a strong predictor of condition, larval history and lipid content increases prior to metamorphosis may translate to higher condition among smaller juvenile fishes [64–66]. We found a growth rate effect on fish $\delta^{15}\text{N}$ values, but no relationship between growth rate and $\delta^{13}\text{C}$ values (electronic supplementary material, table S3). This pattern is consistent with controlled dietary studies where fish growth rate has been altered within captive Atlantic salmon (*Salmo salar*) and summer flounder (*Paralichthys dentatus*) which found depletion in $\delta^{15}\text{N}$ values as growth rates increased [67,68]. The most likely explanation for this pattern is that increasing fish growth rate is accompanied by greater nitrogen use efficiency, influencing fish tissue $\delta^{15}\text{N}$ values [67]. This finding suggests that $\delta^{15}\text{N}$ variation in *Chromis fieldi* is driven primarily by metabolic processes and growth rate changes, rather than coral reef primary production gradients.

Isotopic niche area provides information on the trophic niche occupied by a species [38]. In general, increases in system productivity will result in a more trophically complex ecosystem, thus increasing trophic niche size [69]. This pattern has been observed within planktivorous fish across a strong north–south gradient of oceanic primary production in the Southern Line Islands, where trophic niche expanded with increasing nearshore production [70]. While larger at moderate depths, we found differences in isotopic niche area between depths were not statistically significant (figure 3). By contrast, significant differences in isotopic niche size were observed when samples were grouped by atoll, providing evidence of spatial variation in the ecological niche occupied by planktivorous fish at scales of greater than 150 km (figure 4). The larger isotopic niche at shallow depths within Egmont Atoll (figure 4) is consistent with bathymetry and fine-scale oceanographic processes concentrating zooplankton towards the surface at this location, in a reversal of the general depth pattern. Similar context-specific oceanographic regimes which reverse or homogenize expected trophic zonation across depths have previously been recorded in the central Pacific [24].

The limitations to this study include the restricted depth range of sampling due to diving safety restrictions in a remote location. Goldstein *et al.* [29] examined damselfish growth between shallow (less than 10 m), deep shelf (20–30 m) and mesophotic (60–70 m) reef sites in the Florida Keys, and found significant differences only between shallow and mesophotic depths. Although we characterized surface zooplankton communities across sites, targeted sampling of zooplankton within

specific depth ranges would facilitate testing the hypothesis that these communities differ with increasing proximity to deep water nutrient sources. Finally, although we used the highest resolution of publicly available satellite data to derive chlorophyll-*a* values as a proxy of primary production within the photic zone, we currently lack detailed site-level physical data recording water movements and nutrient concentration across depths to quantify the intensity of processes transporting nutrient-enriched water onto reef slopes. These data would allow a more accurate analysis of the influence of allochthonous nutrient sources on reef fish community growth and condition, and how these vary seasonally within this monsoon-dominated system.

The predicted relationship of higher fish growth rate and depleted $\delta^{15}\text{N}$ values with increasing depth was not observed within our dataset, indicating that any influence of deep water nutrient input on these variables is not detectable in the planktivorous fish *Chromis fieldi* in the shallow to moderate depths we examined (10–17.5 m). Nonetheless, we provide evidence that sites which are ‘hotspots’ of high primary production can influence relationships with planktivore isotopic composition ($\delta^{13}\text{C}$) and condition (C:N ratio), and we found that planktivore trophic niche area differs between shallow and moderate depths within atoll reef systems. While the importance of energetic contributions from external sources to coral reef ecosystems is increasingly evident [5,7,62,63,71], our results show how expected broad-scale patterns can be altered by site-specific variation in physical characteristics influencing planktonic food chains.

Ethics. Ethical approval to conduct fish sampling and euthanasia was given by the ethics committee of the College of Science and Engineering Bangor University. A permit to carry out research was provided by the British Indian Ocean Territory Administration (Ref: BPMS Reef 2 Project 2 2019).

Data accessibility. The pre-registered Stage 1 report can be found on the Open Science Framework at the following link: <https://osf.io/bgqk/>. The code for data analysis and datasets used can be found in the OSF project link: <https://osf.io/6wjsq/>. The raw isotope and otolith growth datasets have been submitted to the Dryad Digital Repository, at the following link: <https://doi.org/10.5061/dryad.q83bk3jkt>.

The data are provided in the electronic supplementary material [72].

Authors' contributions. R.C.R.: formal analysis, investigation, writing—original draft and writing—review and editing; A.H.: conceptualization and writing—review and editing; B.M.T.: investigation and writing—review and editing; J.N.S.: formal analysis and writing—review and editing; M.D.F.: conceptualization and writing—review and editing; L.K.S.: investigation; G.J.W.: conceptualization and writing—review and editing; J.R.T.: funding acquisition and project administration.

All authors gave final approval for publication and agreed to be held accountable for the work performed therein.

Conflict of interest declaration. We declare we have no competing interests.

Funding. Fieldwork was supported by the Fondation Bertarelli.

Acknowledgements. We thank the captain and crew of the Grampian Frontier for their assistance during fieldwork. We also acknowledge the support given to the expedition by the British Indian Ocean Territory Administration. We would like to thank Susan Allender for sampling advice and laboratory assistance.

References

- Rädecker N, Pogoreutz C, Voolstra CR, Wiedenmann J, Wild C. 2015 Nitrogen cycling in corals: the key to understanding holobiont functioning? *Trends Microbiol.* **23**, 490–497. (doi:10.1016/j.tim.2015.03.008)
- Goeij Jd, Oevelen Dv, Vermeij MJA, Osinga R, Middelburg JJ, Goeij Ad, Admiraal W. 2013 Surviving in a marine desert: the sponge loop retains resources within coral reefs. *Science* **342**, 108–110. (doi:10.1126/science.1241981)
- Lesser MP, Falcón LI, Rodríguez-Román A, Enríquez S, Hoegh-Guldberg O, Iglesias-Prieto R. 2007 Nitrogen fixation by symbiotic cyanobacteria provides a source of nitrogen for the scleractinian coral *Montastraea cavemosa*. *Mar. Ecol. Prog. Ser.* **346**, 143–152. (doi:10.3354/meps07008)
- Hamner WM, Jones MS, Carleton JH, Hauri IR, Williams D. 1988 Zooplankton, planktivorous fish, and water currents on a windward reef face: great barrier reef, Australia. *Bullet. Mar. Sci.* **42**, 459–479.
- Gove JM *et al.* 2016 Near-island biological hotspots in barren ocean basins. *Nat. Commun.* **7**, 1–8. (doi:10.1038/ncomms10581)
- Hanson KM, Schnarr EL, Leichter JJ. 2016 Non-random feeding enhances the contribution of oceanic zooplankton to the diet of the planktivorous coral reef fish *Dascyllus flavicaudus*. *Mar. Biol.* **163**, 77. (doi:10.1007/s00227-016-2849-3)
- Morais RA, Bellwood DR. 2019 Pelagic subsidies underpin fish productivity on a degraded coral reef. *Curr. Biol.* **29**, 1521–1527.e6. (doi:10.1016/j.cub.2019.03.044)
- Fabricius KE. 2005 Effects of terrestrial runoff on the ecology of corals and coral reefs: review and synthesis. *Mar. Pollut. Bull.* **50**, 125–146. (doi:10.1016/j.marpolbul.2004.11.028)
- Graham NAJ, Wilson SK, Carr P, Hoey AS, Jennings S, MacNeil MA. 2018 Seabirds enhance coral reef productivity and functioning in the absence of invasive rats. *Nature* **559**, 250–253. (doi:10.1038/s41586-018-0202-3)
- Leichter JJ, Stewart HL, Miller SL. 2003 Episodic nutrient transport to Florida coral reefs. *Limnol. Oceanogr.* **48**, 1394–1407. (doi:10.4319/lo.2003.48.4.1394)
- Aston EA, Williams GJ, Green JAM, Davies AJ, Wedding LM, Gove JM, Jouffray JB, Jones TT, Clark J. 2019 Scale-dependent spatial patterns in benthic communities around a tropical island seascape. *Ecography* **42**, 578–590. (doi:10.1111/ecog.04097)
- Gove JM, Merrifield MA, Brainard RE. 2006 Temporal variability of current-driven upwelling at Jarvis Island. *J. Geophys. Res.* **111**, C12011. (doi:10.1029/2005JC003161)
- Reid EC, DeCarlo TM, Cohen AL, Wong GTF, Lentz SJ, Safaie A, Hall A, Davis KA. 2019 Internal waves influence the thermal and nutrient environment on a shallow coral reef. *Limnol. Oceanogr.* **64**, 1949–1965. (doi:10.1002/lno.11162)

14. Green RH, Jones NL, Rayson MD, Lowe RJ, Bluteau CE, Ivey GN. 2019 Nutrient fluxes into an isolated coral reef atoll by tidally driven internal bores. *Limnol. Oceanogr.* **64**, 461–473. (doi:10.1002/lno.11051)
15. Carter GS, Gregg MC. 2006 Persistent near-diurnal internal waves observed above a site of M_2 barotropic-to-baroclinic conversion. *J. Phys. Oceanogr.* **36**, 1136–1147. (doi:10.1175/JPO2884.1)
16. Wolanski E, Delesalle B. 1995 Upwelling by internal waves, Tahiti, French Polynesia. *Cont. Shelf Res.* **15**, 357–368. (doi:10.1016/0278-4343(93)E0004-R)
17. Letessier TB, Cox MJ, Meeuwij JJ, Boersch-Supan PH, Brierley AS. 2016 Enhanced pelagic biomass around coral atolls. *Mar. Ecol. Prog. Ser.* **546**, 271–276. (doi:10.3354/meps11675)
18. Leichter JJ, Stokes MD, Hench JL, Witting J, Washburn L. 2012 The island-scale internal wave climate of Moorea, French Polynesia. *J. Geophys. Res.* **117**, 6008. (doi:10.1029/2012JC007949)
19. Lowe RJ, Falter JL. 2015 Oceanic forcing of coral reefs. *Annu. Rev. Mar. Sci.* **7**, 43–66. (doi:10.1146/annurev-marine-010814-015834)
20. Wyatt ASJ, Leichter JJ, Toth LT, Miyajima T, Aronson RB, Nagata T. 2020 Heat accumulation on coral reefs mitigated by internal waves. *Nat. Geosci.* **13**, 28–34. (doi:10.1038/s41561-019-0486-4)
21. Fox MD, Williams GJ, Johnson MD, Radice VZ, Zgliczynski BJ, Kelly ELA, Rohwer FL, Sandin SA, Smith JE. 2018 Gradients in primary production predict trophic strategies of mixotrophic corals across spatial scales. *Curr. Biol.* **28**, 3355–3363.e4. (doi:10.1016/j.cub.2018.08.057)
22. Radice VZ, Hoegh-Guldberg O, Fry B, Fox MD, Dove SG. 2019 Upwelling as the major source of nitrogen for shallow and deep reef-building corals across an oceanic atoll system. *Funct. Ecol.* **33**, 1120–1134. (doi:10.1111/1365-2435.13314)
23. Grottoli AG, Rodrigues LJ, Palardy JE. 2006 Heterotrophic plasticity and resilience in bleached corals. *Nature* **440**, 1186–1189. (doi:10.1038/nature04565)
24. Williams GJ *et al.* 2018 Biophysical drivers of coral trophic depth zonation. *Mar. Biol.* **165**, 60. (doi:10.1007/s00227-018-3314-2)
25. Wyatt ASJ, Lowe RJ, Humphries S, Waite AM. 2013 Particulate nutrient fluxes over a fringing coral reef: source-sink dynamics inferred from carbon to nitrogen ratios and stable isotopes. *Limnol. Oceanogr.* **58**, 409–427. (doi:10.4319/lo.2013.58.1.0409)
26. McMahon KW, Thorrold SR, Houghton LA, Berumen ML. 2016 Tracing carbon flow through coral reef food webs using a compound-specific stable isotope approach. *Oecologia* **180**, 809–821. (doi:10.1007/s00442-015-3475-3)
27. Davis JP, Pitt KA, Fry B, Connolly RM. 2015 Stable isotopes as tracers of residency for fish on inshore coral reefs. *Estuarine Coastal Shelf Sci.* **167**, 368–376. (doi:10.1016/j.ecss.2015.10.013)
28. Bourg BL, Letourneur Y, Bänaru D, Blanchot J, Chevalier C, Mou-Tham G, Lebreton B, Pagano M. 2018 The same but different: stable isotopes reveal two distinguishable, yet similar, neighbouring food chains in a coral reef. *J. Mar. Biol. Assoc. UK* **98**, 1589–1597. (doi:10.1017/S0025315417001370)
29. Goldstein ED, D'Alessandro EK, Reed J, Sponaugle S. 2016 Habitat availability and depth-driven population demographics regulate reproductive output of a coral reef fish. *Ecosphere* **7**, e01542. (doi:10.1002/ecs2.1542)
30. MacDonald C, Bridge TCL, McMahon KW, Jones GP. 2019 Alternative functional strategies and altered carbon pathways facilitate broad depth ranges in coral-obligate reef fishes. *Funct. Ecol.* **33**, 1962–1972. (doi:10.1111/1365-2435.13400)
31. Wyatt ASJ, Waite AM, Humphries S. 2012 Stable isotope analysis reveals community-level variation in fish trophodynamics across a fringing coral reef. *Coral Reefs* **31**, 1029–1044. (doi:10.1007/s00338-012-0923-y)
32. Zgliczynski BJ, Williams GJ, Hamilton SL, Cordner EG, Fox MD, Eynaud Y, Michener RH, Kaufman LS, Sandin SA. 2019 Foraging consistency of coral reef fishes across environmental gradients in the central Pacific. *Oecologia* **191**, 433–445. (doi:10.1007/s00442-019-04496-9)
33. Goldstein ED, D'Alessandro EK, Sponaugle S. 2017 Fitness consequences of habitat variability, trophic position, and energy allocation across the depth distribution of a coral-reef fish. *Coral Reefs* **36**, 957–968. (doi:10.1007/s00338-017-1587-4)
34. Samoilyis M, Roche R, Koldewey H, Turner J. 2018 Patterns in reef fish assemblages: insights from the Chagos Archipelago. *PLoS ONE* **13**, e0191448. (doi:10.1371/journal.pone.0191448)
35. Randall JE, DiBattista JD. 2013 A new species of damselfish (Pomacentridae) from the Indian Ocean. *Aqua* **19**, 17.
36. Post DM, Layman CA, Arrington DA, Takimoto G, Quattrochi J, Montaña CG. 2007 Getting to the fat of the matter: models, methods and assumptions for dealing with lipids in stable isotope analyses. *Oecologia* **152**, 179–189. (doi:10.1007/s00442-006-0630-x)
37. Skinner MM, Martin AA, Moore BC. 2016 Is lipid correction necessary in the stable isotope analysis of fish tissues? *Rapid Commun. Mass Spectrom.* **30**, 881–889. (doi:10.1002/rcm.7480)
38. Jackson AL, Inger R, Parnell AC, Bearhop S. 2011 Comparing isotopic niche widths among and within communities: SIBER – Stable Isotope Bayesian Ellipses in R. *J. Anim. Ecol.* **3**, 595–602. (doi:10.1111/j.1365-2656.2011.01806.x)
39. Taylor BM, Gourley J, Trianni MS. 2017 Age, growth, reproductive biology and spawning periodicity of the forktail rabbitfish (*Siganus argenteus*) from the Mariana Islands. *Mar. Freshwater Res.* **68**, 1088–1097. (doi:10.1071/MF16169)
40. Morais RA, Bellwood DR. 2018 Global drivers of reef fish growth. *Fish Fish.* **19**, 874–889. (doi:10.1111/faf.12297)
41. Behrenfeld MJ, Falkowski PG. 1997 A consumer's guide to phytoplankton primary productivity models. *Limnol. Oceanogr.* **42**, 1479–1491. (doi:10.4319/lo.1997.42.7.1479)
42. Gall M, Hawes I, Boyd P. 1999 Predicting rates of primary production in the vicinity of the Subtropical Convergence east of New Zealand. *New Zealand J. Mar. Freshw. Res.* **33**, 443–455. (doi:10.1080/00288330.1999.9516890)
43. Croll DA, Marinovic B, Benson S, Chavez FP, Black N, Ternullo R, Tershry BR. 2005 From wind to whales: trophic links in a coastal upwelling system. *Mar. Ecol. Prog. Ser.* **289**, 117–130. (doi:10.3354/meps289117)
44. Hazen EL, Suryan RM, Santora JA, Bograd SJ, Watanuki Y, Wilson RP. 2013 Scales and mechanisms of marine hotspot formation. *Mar. Ecol. Prog. Ser.* **487**, 177–183. (doi:10.3354/meps10477)
45. Gove JM, Williams GJ, McManus MA, Heron SF, Sandin SA, Vetter OJ, Foley DG. 2013 Quantifying climatological ranges and anomalies for Pacific coral reef ecosystems. *PLoS ONE* **8**, e61974. (doi:10.1371/journal.pone.0061974)
46. Amante C, Eakins BW. 2009 ETOPO1 arc-minute global relief model: procedures, data sources and analysis. *NOAA Tech. Memo. NESDIS NGDC-24*, 19 pp. (doi:10.7289/V5C8276M)
47. Bulgarelli B, Zibordi G. 2018 On the detectability of adjacency effects in ocean color remote sensing of mid-latitude coastal environments by SeaWiFS, MODIS-A, MERIS, OLCI, OLI and MSI. *Remote Sens. Environ.* **209**, 423–438. (doi:10.1016/j.rse.2017.12.021)
48. Chami M, Lenot X, Guillaume M, Lafrance B, Briottet X, Minghelli A, Jay S, Deville Y, Serfaty V. 2019 Analysis and quantification of seabed adjacency effects in the subsurface upwelling radiance in shallow waters. *Opt. Express* **27**, A319–A338. (doi:10.1364/OE.27.00A319)
49. O'Reilly JE, Maritorena S, Mitchell BG, Siegel DA, Gardner KL, Garver SA, Kahru M, McClain C. 1998 Ocean color chlorophyll algorithms for SeaWiFS. *J. Geophys. Res.* **103**, 24 937–24 953. (doi:10.1029/98JC02160)
50. Bailey SW, Werdell PJ. 2006 A multi-sensor approach for the on-orbit validation of ocean color satellite data products. *Remote Sens. Environ.* **102**, 12–23. (doi:10.1016/j.rse.2006.01.015)
51. Barnes BB, Garcia R, Hu C, Lee Z. 2018 Multi-band spectral matching inversion algorithm to derive water column properties in optically shallow waters: an optimization of parameterization. *Remote Sens. Environ.* **204**, 424–438. (doi:10.1016/j.rse.2017.10.013)
52. Benjamini Y, Hochberg Y. 1995 Controlling the false discovery rate: a practical and powerful approach to multiple testing. *J. R. Stat. Soc.* **57**, 289–300. (doi:10.1111/j.2517-6161.1995.tb02031.x)
53. Sheppard C. 2009 Large temperature plunges recorded by data loggers at different depths on an Indian Ocean atoll: comparison with satellite data and relevance to coral refuges. *Coral Reefs* **28**, 399–403. (doi:10.1007/s00338-009-0476-x)
54. Harris JL, Hosegood P, Robinson E, Embling CB, Hailbourne S, Stevens GMW. 2021 Fine-scale oceanographic drivers of reef manta ray (*Mobula alfredi*) visitation patterns at a feeding aggregation site. *Ecol. Evol.* **11**, 4588–4604. (doi:10.1002/ece3.7357)
55. Friedlander AM, Sandin SA, DeMartini EE, Sala E. 2010 Spatial patterns of the structure of reef fish assemblages at a pristine atoll in the central Pacific. *Mar. Ecol. Prog. Ser.* **410**, 219–231. (doi:10.3354/meps08634)

56. Bejarano I, Appeldoorn RS, Nemeth M. 2014 Fishes associated with mesophotic coral ecosystems in La Parguera, Puerto Rico. *Coral Reefs* **33**, 313–328. (doi:10.1007/s00338-014-1125-6)
57. Goldstein ED, D'Alessandro EK, Sponaugle S. 2016 Demographic and reproductive plasticity across the depth distribution of a coral reef fish. *Sci. Rep.* **6**, 34077. (doi:10.1038/srep34077)
58. DiBattista JD *et al.* 2021 Growth patterns of specialized reef fishes distributed across the Red Sea to Gulf of Aden. *Environ. Biol. Fish* **104**, 967–976. (doi:10.1007/s10641-021-01129-0)
59. McClanahan TR, Graham NAJ. 2015 Marine reserve recovery rates towards a baseline are slower for reef fish community life histories than biomass. *Proc. R. Soc. B* **282**, 20151938. (doi:10.1098/rspb.2015.1938)
60. McClanahan TR, Friedlander AM, Graham NAJ, Chabanet P, Bruggemann JH. 2021 Variability in coral reef fish baseline and benchmark biomass in the central and western Indian Ocean provinces. *Aquat. Conserv.* **31**, 28–42. (doi:10.1002/aqc.3448)
61. Ferretti F, Curmick D, Liu K, Romanov EV, Block BA. 2018 Shark baselines and the conservation role of remote coral reef ecosystems. *Sci. Adv.* **4**, eaaq0333. (doi:10.1126/sciadv.aaq0333)
62. Heenan A, Williams GJ, Williams ID. 2020 Natural variation in coral reef trophic structure across environmental gradients. *Front. Ecol. Environ.* **18**, 69–75. (doi:10.1002/fee.2144)
63. Skinner C, Mill AC, Fox MD, Newman SP, Zhu Y, Kuhl A, Polunin NVC. 2021 Offshore pelagic subsidies dominate carbon inputs to coral reef predators. *Sci. Adv.* **7**, eabf3792. (doi:10.1126/sciadv.abf3792)
64. Hamilton SL, Regetz J, Warner RR. 2008 Postsettlement survival linked to larval life in a marine fish. *Proc. Natl Acad. Sci. USA* **105**, 1561–1566. (doi:10.1073/pnas.0707676105)
65. Shima JS, Swearer SE. 2010 The legacy of dispersal: larval experience shapes persistence later in the life of a reef fish. *J. Anim. Ecol.* **79**, 1308–1314. (doi:10.1111/j.1365-2656.2010.01733.x)
66. Dingeldein AL, White JW. 2016 Larval traits carry over to affect post-settlement behaviour in a common coral reef fish. *J. Anim. Ecol.* **85**, 903–914. (doi:10.1111/1365-2656.12506)
67. Trueman CN, McGill RAR, Guyard PH. 2005 The effect of growth rate on tissue-diet isotopic spacing in rapidly growing animals. An experimental study with Atlantic salmon (*Salmo salar*). *Rapid Commun. Mass Spectrom.* **19**, 3239–3247. (doi:10.1002/rcm.2199)
68. Buchheister A, Latour RJ. 2010 Turnover and fractionation of carbon and nitrogen stable isotopes in tissues of a migratory coastal predator, summer flounder (*Paralichthys dentatus*). *Can. J. Fish. Aquat. Sci.* **67**, 445–461. (doi:10.1139/F09-196)
69. Lesser JS, James WR, Stallings CD, Wilson RM, Nelson JA. 2020 Trophic niche size and overlap decreases with increasing ecosystem productivity. *Oikos* **129**, 1303–1313. (doi:10.1111/oik.07026)
70. Miller SD, Zgliczynski BJ, Fox MD, Kaufman LS, Michener RH, Sandin SA, Hamilton SL. 2019 Niche width expansion of coral reef fishes along a primary production gradient in the remote central Pacific. *Mar. Ecol. Prog. Ser.* **625**, 127–143. (doi:10.3354/meps13023)
71. Williams ID, Baum JK, Heenan A, Hanson KM, Nadon MO, Brainard RE. 2015 Human, oceanographic and habitat drivers of central and western Pacific coral reef fish assemblages. *PLoS ONE* **10**, e0120516. (doi:10.1371/journal.pone.0120516)
72. Roche RC, Heenan A, Taylor BM, Schwarz JN, Fox MD, Southworth LK, Williams GJ, Turner JR. 2022 Data from: Linking variation in planktonic primary production to coral reef fish growth and condition. FigShare. (doi:10.6084/m9.figshare.c.6156452)